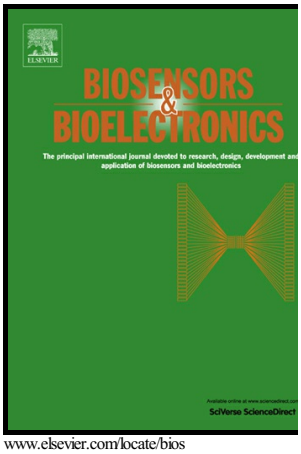

Facile fabrication of an aptasensor for thrombin based on graphitic carbon nitride/TiO_2 with High visible-light photoelectrochemical activity

Dawei Fan, Cuijuan Guo, Hongmin Ma, Di Zhao, Yina Li, Dan Wu, Qin Wei

www.elsevier.com/locate/bios

PII: S0956-5663(15)30353-5
DOI: http://dx.doi.org/10.1016/j.bios.2015.08.029
Reference: BIOS7925

To appear in: *Biosensors and Bioelectronic*

Received date: 26 June 2015
Revised date: 10 August 2015
Accepted date: 14 August 2015

Cite this article as: Dawei Fan, Cuijuan Guo, Hongmin Ma, Di Zhao, Yina Li Dan Wu and Qin Wei, Facile fabrication of an aptasensor for thrombin based or graphitic carbon nitride/TiO_2 with High visible-light photoelectrochemica activity, *Biosensors and Bioelectronic* http://dx.doi.org/10.1016/j.bios.2015.08.029

Facile fabrication of an aptasensor for thrombin based on graphitic carbon nitride/TiO_2 with high visible-light photoelectrochemical activity

Dawei Fan, Cuijuan Guo, Hongmin Ma, Di Zhao, Yina Li, Dan Wu*, Qin Wei

Key Laboratory of Chemical Sensing & Analysis in Universities of Shandong (University of Jinan), School of Chemistry and Chemical Engineering, University of Jinan, Jinan 250022, China

Corresponding author:

*E-mail address: wudan791108@163.com, Tel: +86-0531-82767872

ABSTRACT

A novel aptasensor for thrombin with high visible-light activity was facilely fabricated based on graphitic carbon nitride/TiO_2 (g-C_3N_4/TiO_2) photoelectrochemical (PEC) composite. Crystallization of TiO_2 nanoparticles (NPs) and their strong interaction with g-C_3N_4 sheet were confirmed by high-resolution transmission electron microscope (HR-TEM), both of which contributed to the high photocurrent intensity under visible-light irradiation. Carboxyl functionalized thrombin aptamers were first successfully bound to the g-C_3N_4/TiO_2 modified electrode as proven by photoelectrochemical test and electrochemical impedance spectroscopy (EIS) analysis. Ascorbic acid was utilized as the electron donor for scavenging photo-generated holes and inhibiting light driven electron-hole pair recombination. The specific recognition between thrombin aptamer and thrombin led to the linear decrease of photocurrent with the increase of logarithm of thrombin concentration in the range of 5.0×10^{-13} mol L^{-1} to 5.0×10^{-9} mol L^{-1} with a detection limit of 1.2×10^{-13} mol L^{-1}. This

proposed low-cost, convenient and sensitive aptasensor showed promising applications in biosensor and photoelectrochemical analysis.

Keywords: Aptasensor; g-C_3N_4/TiO_2; Thrombin; Visible-light; Photoelectrochemical activity

1. Introduction

Photoelectrochemical (PEC) sensor is a promising detection technology based on the relationship between the changes of photovoltage/photocurrent and the concentration of target analyte during a PEC reaction. Due to its high selectivity and sensitivity, short response time, minimal sample consumption and low background signals, photoelectrical sensor has become a powerful technology in many fields such as medical diagnostics, food safety, target detection, and environmental science (Brown et al., 1992; Freeman et al., 2013; Yue et al., 2013). Aptamers are oligonucleotides (DNA or RNA) artificially synthesized using an in vitro selection method named SELEX (Ellington and Szostak, 1990; Hermann and Patel, 2000). Aptamers exhibit many advantages such as stability of secondary structures, ease of production and storage, high specificity and affinity to target analytes, and good reproducibility. A PEC aptasensor can be constructed tactfully by combining the advantages of photoelectric analysis and aptamers (Zhao et al., 2014).

Photoelectric materials with high PEC activities are the foundation of sensitive target detection. PEC sensors based on TiO_2 have been widely fabricated on account of their superior chemical stability, high loading capacity, good PEC activity, non-toxicity, etc (Hoffmann et al., 1995; Thompson and Yates Jr, 2006; Linsebigler et

al., 1995). However, TiO_2 is only UV active at wavelengths lower than 387.5 nm because of its wide bandgap of 3.2 eV, which limits its practical applications. In recent years, significant effort has been made to extend the PEC activity of TiO_2 to visible-light range. Such effort includes quantum dot sensitization (Yue et al., 2013), doping of metallic elements (Inturi et al., 2014; Li et al., 2015) or nonmetallic elements (Asahi et al., 2001; Valentin et al., 2005; Tang and Li, 2008), and preparation of composite based on TiO_2 (Rajh et al., 2014).

Graphitic carbon nitride (g-C_3N_4) is a new class of semiconductor that is chemically stable and easy to prepare. It has a visible-light driven bandgap of 2.69 eV. g-C_3N_4 has emerged as a good photoelectric material for splitting water (Wang et al., 2009b; Schwinghammer et al., 2014), degrading organic pollutants (Wang et al., 2012), producing electrochemiluminescence (Li et al., 2014b) and constructing photoelectrochemical immunosensors (Li et al., 2014a). However, high recombination rate of photo-generated electron-hole pairs is the bottleneck that impacts the photoelectric efficiency of g-C_3N_4 in practical applications. For use as ultrasensitive sensors, the photo-to-current conversion efficiency of g-C_3N_4 needs to be improved. The formation of heterojunctions has been considered as an efficient photo-generated electron/hole transfer from g-C_3N_4 to TiO_2 substrate. g-C_3N_4/TiO_2 nanofibres (Zhang et al., 2014), hybrid C_3N_4/TiO_2 prepared via ball milling method (Zhou et al., 2015), nanosheets (Tong et al., 2015) and Z-scheme g-C_3N_4/TiO_2 photocatalysts (Yu et al., 2013) have been studied for the degradation of organic pollutants and purification of indoor air.

To the best of our knowledge, g-C_3N_4/TiO_2 composite has not been utilized in the area of PEC aptasensors. In this paper, a novel g-C_3N_4/TiO_2 composite was prepared by the one-pot method. The strong interactions between TiO_2 nanoparticles (NPs) and the g-C_3N_4 sheet were confirmed by HR-TEM and the PEC test. Furthermore, the stable, highly active and efficient immobilization of aptamers or biomolecules onto the surface of sensor is also very crucial in the fabrication of PEC sensors, which may influence the test level and effect of the sensor. EIS analysis proved successful incorporation of carboxyl functionalized aptamers onto the g-C_3N_4/TiO_2 modified electrode via strong coordination interaction of TiO_2-carboxyl binding (Anderson et al., 1979; Eu et al., 2007; Tu et al., 2009; Liu et al., 2015). Thrombin is an important physiological protease generated from the hydrolase of serine. The concentration and activity of thrombin are crucial indicators for blood coagulation, and the formation, progression and early diagnosis of tumors. The specific recognition between thrombin aptamer and thrombin is the basis for the new g-C_3N_4/TiO_2 PEC aptasensor, which may find further applications in sensing and diagnostics.

2. Experimental

2.1. Materials and apparatus

Thrombin was obtained from Sigma-Aldrich Chemical Co. (St. Louis, MO, USA). Thrombin aptamer (TBA): 5′-COOH-$(CH_2)_{10}$-GGT TGG TGT GGT TGG-3′ was purchased from TaKaRa (Dalian, China). The details are shown in Electronic Supplementary Information (ESI†).

All PEC experiments were performed on a CHI760E electrochemical workstation

(Chenhua Instrument Shanghai Co., Ltd, China). The details are shown in ESI†.

2.2. Preparation of C_3N_4/TiO_2 composite

C_3N_4 was synthesized as described previously with slight modifications (Cheng et al., 2012). The details are shown in ESI†. Novel C_3N_4/TiO_2 hybrid composites were prepared by varying the amounts of bulk C_3N_4 in the preparation procedure as shown in Fig. 1A. Briefly, a certain amount of C_3N_4 powder, which was sonicated beforehand in 30 mL of absolute ethanol for 1 h, was added into a conical flask containing 0.02 mol tetrabutyl orthotitanate (TBOT). Then 10 mL ultrapure water was added into the TBOT and C_3N_4 solution dropwise under magnetic stirring at 30 ºC. After 2 h, the solution was transferred into a Teflon-lined autoclave and maintained at 200 °C for 10 h. The resulting precipitates were collected and washed thoroughly with absolute ethanol and ultrapure water for three cycles, respectively, and then dried in a vacuum at 50 °C for 24 h. As the control, pure TiO_2 was synthesized under the same processing condition without C_3N_4 (Huang et al., 2013). The weight percentages of C_3N_4 in C_3N_4/TiO_2 hybrid composites were controlled to be 0.5%, 1%, 2%, 3%, 5%, and 7%. A series of products were collected and ground into powder for further use.

2.3. Fabrication of PEC aptasensor

Schematic illustration of PEC aptasensor fabrication process is depicted in Fig. 1B. ITO substrates were cleaned by immersion for 30 min at 50 ºC in a series of ultrasonically agitated solvents (H_2O, acetone, ethanol, H_2O) and dried under a nitrogen stream. A 10 μL of 4 mg mL^{-1} C_3N_4/TiO_2 solution was sonicated in water for 30 min and dropped onto the pre-cleaned ITO electrode, forming a film. The film was

dried under an infrared lamp, followed by calcination at 450 °C for 30 min in a muffle oven and naturally cooling to room temperature.

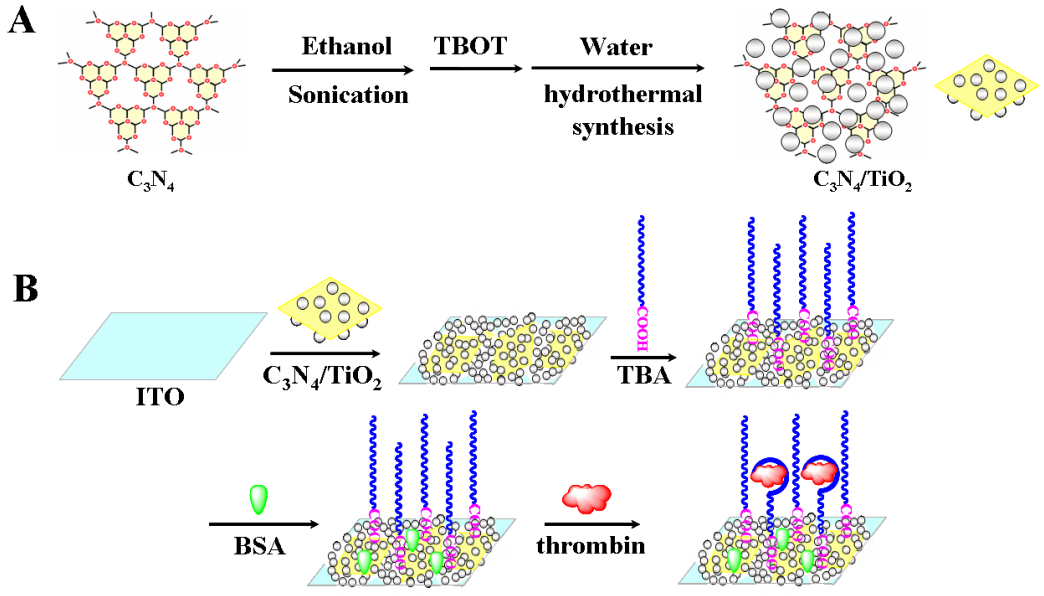

Fig. 1. Schematic illustration of C_3N_4/TiO_2 preparation (A) and the PEC aptasensor fabrication process (B).

A 6 μL of 5 μmol L^{-1} thrombin aptamer (TBA) solution was applied to the surface of the ITO/(C_3N_4/TiO_2) electrode and let react for 1 h at room temperature. Binding of TBA was achieved via the covalent bond formed between carboxyl group of TBA and TiO_2 (Anderson et al., 1979). After rinsing, the unreacted active sites on the electrode surface were deactivated by 6 μL of 0.1% bovine serum albumin (BSA) solution for 1 h at 4 ºC and then washed thoroughly. After that, 6 μL of thrombin solutions with different concentrations were incubated for 40 min at 37 ºC and immobilized on the modified electrode surface through the specific recognition affinity reaction. The unbound thrombin was washed away, the prepared ITO/(C_3N_4/TiO_2)/TBA/BSA/thrombin electrodes were stored at 4 ºC until use.

3. Results and discussion

3.1. Morphology and spectroscopic characterizations of TiO_2, C_3N_4 and C_3N_4/TiO_2 composite

TEM and HR-TEM were used to characterize the sizes and morphologies of TiO_2, C_3N_4 and C_3N_4/TiO_2 hybrid composites. Fig. 2A shows the irregular and agglomerated spherical TiO_2 NPs with an average diameter of ~8.3 nm. As shown in Fig. 2B, C_3N_4 has a graphitic-like nanosheet structure. Fig. 2C and 2D display the structures of 1%C_3N_4/TiO_2 and 3%C_3N_4/TiO_2 composites, in which TiO_2 NPs grow with C_3N_4 nanosheet synergistically. Red arrows in the images (Fig. 2C, 2D, 2E, 2F) indicate the presence of C_3N_4 sheets. In fact, the interaction between TiO_2 NPs and C_3N_4 nanosheet was so strong that TiO_2 NPs could not be peeled off from the C_3N_4 nanosheet by ultrasonication before TEM and HR-TEM characterization. HR-TEM images (Fig. 2E and inset in Fig. 2E) confirm the clear lattice spacing of ~0.35 nm corresponding to the (101) lattice plane of anatase TiO_2. Excellent crystallization of TiO_2 NPs and their strong interaction with C_3N_4 demonstrate the formation of heterojunctions between TiO_2 and C_3N_4 in the composites (Xu et al., 2013), which should promote the transfer of the photo-generated electrons.

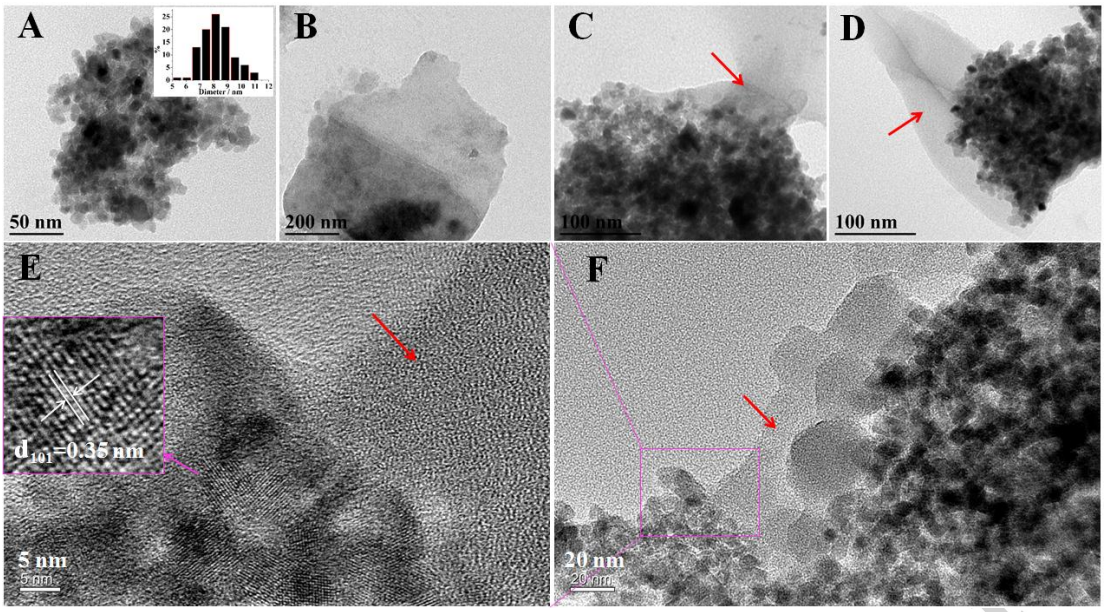

Fig. 2. TEM images of TiO_2 NPs (A), C_3N_4 (B), 1%C_3N_4/TiO_2 (C), and 3%C_3N_4/TiO_2 (D). HR-TEM images of 1%C_3N_4/TiO_2 (E, F). Diameter distribution histograms (inset in A) and (101) crystal plane (inset in E) of TiO_2 NPs. Red arrows in images (C, D, E, F) indicate the presence of C_3N_4 sheets.

Fig. S1 (ESI†) shows the SEM images of modified ITO electrodes with 4 mg mL^{-1} TiO_2, 1%C_3N_4/TiO_2, 3%C_3N_4/TiO_2, and C_3N_4 following calcinations. It can be seen that TiO_2 NPs tend to agglomerate (Fig. S1A), which is in accordance with the TEM image (Fig. 2A). With the addition of C_3N_4, the degrees of agglomeration for 1%C_3N_4/TiO_2 (Fig. S1B) and 3%C_3N_4/TiO_2 (Fig. S1C) decrease slightly with no observable spare g-C_3N_4 nanosheet. This agrees with the analysis of the TEM images (Fig. 2C-2F) that TiO_2 NPs and g-C_3N_4 nanosheet grow synergistically. Fig. S1D shows the nanosheet structure of g-C_3N_4.

Fig. 3A shows the XRD patterns of TiO_2 (before (a) and after calcination (b)), C_3N_4/TiO_2 samples with varied weight percentages of C_3N_4 (0.5% to 7%) (after calcinations (c)-(h)), and C_3N_4 (I). For pure TiO_2, the XRD patterns match well with

the pure anatase TiO_2 (JCPDS Card no. 21-1272). Diffraction peaks at 25.4°, 37.9°, 48.0°, 54.2°, 54.9° and 62.7° are indexed to the (101), (004), (200), (105), (211) and (204) facets of the anatase TiO_2. Compared with TiO_2 NPs before calcinations (a), no new peak emerged in the XRD pattern of TiO_2 NPs after calcinations (b), which reveals that no crystal transformation of TiO_2 occurred at 450 °C. On the other hand, two peaks are present in the XRD pattern of pure C_3N_4 shown in Fig. 3A (I), showing improved graphitic-like layer structure of C_3N_4 (Liao et al., 2012; Liu and Zhang, 2013). The characteristic peaks at 13.1° and 27.5° can be assigned to (100) facet diffraction arising from the in-plane repeating motifs of the continuous heptazine network, and to (002) facet caused by the stacking of the conjugated aromatic system, respectively (Sun et al., 2012). As shown in Fig. 3A (c-h), no characteristic peaks of C_3N_4 are observable in C_3N_4/TiO_2 composites, which may be due to the low percentage of C_3N_4 in the composite. In other words, the considerably weak diffraction peaks of C_3N_4 are covered by strong diffraction peaks of TiO_2 NPs.

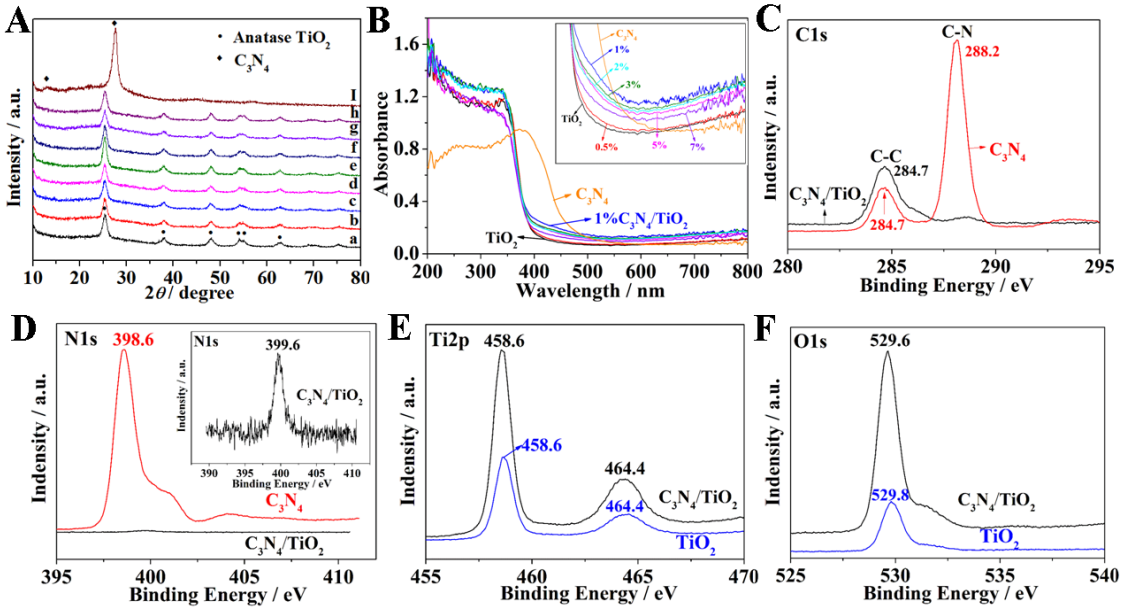

Fig. 3. (A) XRD patterns of TiO_2 before calcinations (a), TiO_2 (b), 0.5%C_3N_4/TiO_2 (c), 1%

C_3N_4/TiO_2 (d), 2%C_3N_4/TiO_2 (e), 3%C_3N_4/TiO_2 (f), 5%C_3N_4/TiO_2 (g), 7%C_3N_4/TiO_2 (h) after calcinations, and C_3N_4 (I). (B) UV-vis diffuse reflectance spectra of C_3N_4, TiO_2 and C_3N_4/TiO_2 with different weight percentages of C_3N_4 ranging from 0.5% to 7%. Inset of (B) shows the magnified area between 350 nm and 800 nm of (B). High-resolution XPS spectra of C1s (C) and N1s (D) for C_3N_4 and 1%C_3N_4/TiO_2 samples, Ti2p (E) and O1s (F) for TiO_2 and 1%C_3N_4/TiO_2. Magnified XPS spectrum of N1s of 1%C_3N_4/TiO_2 is shown in the inset of (D).

Fig. 3B depicts the UV-vis diffuse reflectance spectra of C_3N_4, TiO_2 and C_3N_4/TiO_2. The absorption wavelength of TiO_2 NPs is clearly under 400 nm in the UV range, which is ascribed to the wide bandgap of 3.2 eV (Grätzel et al., 2001), while the absorption wavelength of pure C_3N_4 can reach up to 460 nm as a result of a lower bandgap of 2.69 eV. It can be seen in the insert of (B) that C_3N_4/TiO_2 composites exhibit enhanced absorption in visible-light region from 400 nm to 800 nm in comparison with pure TiO_2 NPs. The absorption intensities are influenced by the weight percentage of C_3N_4 in the composite. These results suggest that C_3N_4 nanosheet may serve as a visible-light sensitizer to drive a reaction on the surface of TiO_2 NPs and possibly influence electron-hole pair formation under irradiation.

The interaction between TiO_2 and C_3N_4 is further characterized by XPS. Fig. 3C shows the high-resolution C1s spectra of C_3N_4 and 1% C_3N_4/TiO_2. It is clear that both samples share two C1s peaks at 284.7 eV and 288.2 eV. The former is assigned to the adventitious hydrocarbon from the XPS instrument itself and the latter one is attributed to carbon atoms from N-C=N_2 coordination (Thomas et al., 2008; Khabashesku et al., 2000). The intensity ratio of the peak at 288.2 eV to the peak at

284.7 eV is much lower in the 1%C_3N_4/TiO_2 sample than in pure C_3N_4, which could be ascribed to the low weight percentage of C_3N_4 in C_3N_4/TiO_2 composite. Fig. 3D depicts the high-resolution N1s XPS spectra of pure C_3N_4 and 1% C_3N_4/TiO_2. The asymmetrical N1s peak is observed in pure C_3N_4 which indicates the coexistence of chemically different N species. The main N1s binding energy located at 398.6 eV is typically attributable to sp^2-hybridized aromatic nitrogen (C=N-C) (Thomas et al., 2008; Yan et al., 2010; Liu et al., 2011). The weak N1s peak centered at 399.6 eV of 1% C_3N_4/TiO_2 (inset of Fig. 3D) is 1 eV higher than that of the pristine C_3N_4 (398.6 eV), which confirms the strong interfacial interaction between C_3N_4 nanosheets and TiO_2 NPs. In Fig. 3E, the peaks at 458.6 eV and 464.4 eV in both pure TiO_2 and 1% C_3N_4/TiO_2 correspond to the binding energies of Ti2p3/2 and Ti2p1/2 of TiO_2, respectively (Reddy et al., 2004). As shown in Fig. 3F, the characteristic binding energy of O1s in 1% C_3N_4/TiO_2 is 529.6 eV, slightly lower than that in TiO_2 (529.8 eV). This shift may be a result of the incorporation into C_3N_4 nanosheets.

3.2. Characterization of the fabricated PEC aptasensor

Ascorbic acid (AA) was employed in the PEC test as the scavenger of photo-generated hole to inhibit electron-hole recombination, promoting electron-hole separation efficiency. The photocurrent-time curves in Fig. 4A show the effect of calcination on the photocurrent response of PEC sensors. The photocurrent responses of TiO_2 (Fig. 4A (a)) and C_3N_4/TiO_2 (Fig. 4A (b)) modified electrodes are both much higher after calcination than before (Fig. 4A (a′) and (b′)). This enhancement in PEC responses can be attributed to firmer immobilization of TiO_2 NPs or C_3N_4/TiO_2 on the

ITO electrodes as a result of calcination.

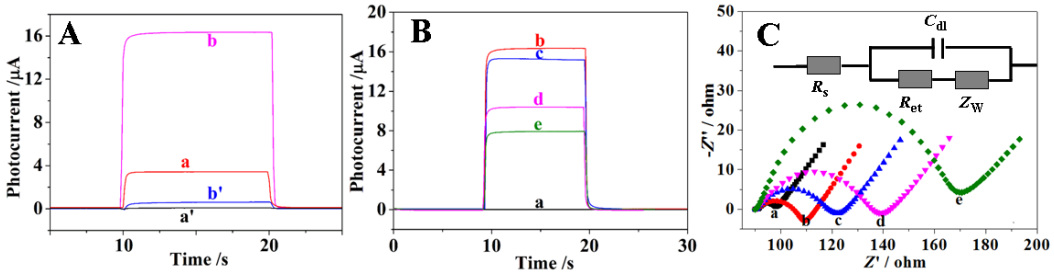

Fig. 4. (A) Photocurrent responses of ITO/TiO_2 (a) and ITO/(1%C_3N_4/TiO_2) (b) modified electrodes after calcinations and ITO/TiO_2 (a′) and ITO/(1%C_3N_4/TiO_2) (b′) modified electrodes before calcinations. (B) Photocurrent responses and (C) EIS Nyquist plots of different modified electrode: (a) ITO, (b) ITO/(1%C_3N_4/TiO_2), (c) ITO/(1%C_3N_4/TiO_2)/TBA, (d) ITO/(1%C_3N_4/TiO_2)/TBA/BSA, (e) ITO/(1%C_3N_4/TiO_2)/TBA/BSA/thrombin, $c_{thrombin}$=1.0 nmol L^{-1}. The applied potential was 0 V. The buffer solution is pH 7.4 PBS with 0.1 mol L^{-1} AA in (A) and (B). The inset in (C) is Randles equivalent circuit.

Time-dependent photocurrent response of each layer of the PEC aptasensor for thrombin is presented in Fig. 4B. No photocurrent was generated for bare ITO under visible light illumination (curve a). On the other hand, calcinated ITO/(1%C_3N_4/TiO_2) electrode showed strong photocurrent of around 16 μA (curve b). With the loading of carboxyl functionalized thrombin aptamer (TBA) onto the 1%C_3N_4/TiO_2 modified ITO electrode, photo-generated electron transfer could be blocked, thus reducing the photocurrent (curve c). When BSA molecules assembled on the (1%C_3N_4/TiO_2)/TBA modified ITO electrode, the photocurrent intensity decreased (curve d). This phenomenon could be due to hampered electron transfer from AA to electrode by the insulating BSA biomolecules, resulting in photo-generated electron-hole recombination. The specific binding of target analyte thrombin to TBA caused a

decrease in photocurrent as shown in curve e ($c_{thrombin}$=1.0 nmol L^{-1}). This achieved the detection of thrombin by the new PEC aptasensor.

Electrochemical impedance spectroscopy (EIS), a tool for evaluating electron transfer resistance (An et al., 2010), was used to characterize the stepwise modification of the electrodes in a 5.0 mM $[Fe(CN)_6]^{3-/4-}$ solution. The semicircle diameter corresponds to the electron transfer resistance value. The EIS Nyquist plots of each step of electrode modification are shown in Fig. 4C. The inset in Fig. 4C is Randles equivalent circuit simulated with ZSimWin software, and the values of them were in Table S1 (ESI†). The circuit includes the resistance of solution (R_s), the double layer capacitance (C_{dl}), the electrode transfer resistance (R_{et}) and the Warburg impedance (Z_W). The modifications of the electrode only affected R_{et}, which was an appropriate signal revealing the interfacial properties of the modified ITO electrodes. Non-modified ITO electrode showed a small semicircle diameter (curve a), implying a low electron transfer resistance. An increase in semicircle diameter can be seen after modification with 1%C_3N_4/TiO_2 (curve b), indicating that the C_3N_4/TiO_2 composite as semiconductor could inhibit the electron transfer of $[Fe(CN)_6]^{3-/4-}$ probe. Subsequent coating by TBA led to further increase of the electron transfer resistance due to their insulation properties (curve c). According to the insulation properties of protein, the semicircle diameters of EIS augmented gradually after sequential modification of BSA (curve d) and thrombin (curve e). The detection of thrombin is therefore achieved.

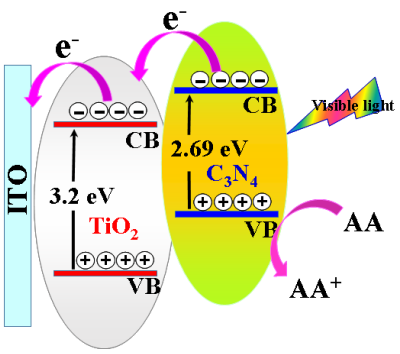

Fig. 5. Schematic illustration of electron transfer of C_3N_4/TiO_2 PEC aptasensor in AA electrolyte.

Based on the above analyses, the mechanism of electron transfer in C_3N_4/TiO_2 PEC aptasensor is proposed in the environment of ascorbic acid (AA) electrolyte (Fig. 5). Photo-generated electrons and holes in pure g-C_3N_4 tend to recombine, resulting in low PEC activity. When C_3N_4/TiO_2 composites are irradiated by visible light, the photo-generated electrons from g-C_3N_4 can transfer from conduction band (CB) of g-C_3N_4 to the CB of TiO_2. It is worth mentioning that the CB and valence band (VB) edges of g-C_3N_4 are higher than those of TiO_2 NPs, which is beneficial for the above transfer process of photo-generated carriers. AA is a kind of excellent electron donor in this PEC aptasensor, which blocks the recombination of photo-generated electrons and holes and meanwhile promotes the electron transfer from CB of TiO_2 NPs to ITO electrode. The specific binding of target analyte thrombin to TBA blocked the electron transfer from AA to C_3N_4/TiO_2 composite and resulted in the recombination of photo-generated holes and electrons, which could explain a decrease in photocurrent. Moreover, the photocurrent intensity decreased gradually with the increase of thrombin concentration. Therefore, the quantitative detection of thrombin is achieved by monitoring the photocurrent decrease after the binding of thrombin.

3.3. Optimization of experimental conditions of C_3N_4/TiO_2 modified electrode

Effects of synthetic conditions for C_3N_4/TiO_2 modified electrode are shown in Fig. S2 (ESI†). The photocurrent intensity of ITO/(C_3N_4/TiO_2) electrode increased with the concentration of C_3N_4 in C_3N_4/TiO_2 from 0%~1% (Fig. S2A). It could be explained that the well-distributed C_3N_4/TiO_2 heterojunctions formed when concentration of C_3N_4 was 1%, which contributed to photocurrent transfer from CB of C_3N_4 to CB of TiO_2. Excess C_3N_4 (>1%) tended to self-assemble (for example, 5%C_3N_4/TiO_2 shown in Fig. S3, ESI†) and formed more recombination centre of photo-generated holes and electrons, reducing the photocurrent intensity. Therefore, 1%C_3N_4/TiO_2 was chosen as the optimal weight percentage of C_3N_4 in C_3N_4/TiO_2 composite for the following experiments.

The concentration of C_3N_4/TiO_2 suspension was studied from 1 mg mL^{-1} to 6 mg mL^{-1} shown in Fig. S2B. It is evident that 4 mg mL^{-1} 1%C_3N_4/TiO_2 suspension generated the highest photocurrent intensity. Increased concentration of C_3N_4/TiO_2 suspension could augment the thickness of the composite film (Kuang et al., 2006), which would form more photoactive materials and enhance light absorption (Li et al., 2012). However, thicker C_3N_4/TiO_2 film could also lead to increased diffusion resistance for electron motion, which causes a decrease in photocurrent intensity (Wang et al., 2009a). Therefore, 4 mg mL^{-1} 1%C_3N_4/TiO_2 suspension was employed as the optimal concentration for subsequent work.

The effect of ascorbic acid is shown in Fig. S2C. The photocurrent intensity reached a maximum value at 0.1 mol L^{-1} AA, which could be ascribed to the saturation of electron donor at an AA concentration higher than 0.1 mol L^{-1}. Thus, 0.1

moL L^{-1} was selected as the optimal concentration of AA.

The effect of pH of the substrate solution on the photocurrent response of the ITO/(C_3N_4/TiO_2) electrode is shown in Fig. S2D. The photocurrent intensity reached the maximum value in the buffer solution of pH 7.4. This pH is similar to physiological pH, which retains the activity of the immobilized protein. pH 7.4 substrate solution was then chosen for the following studies.

3.4. Photoelectrochemical detection of thrombin

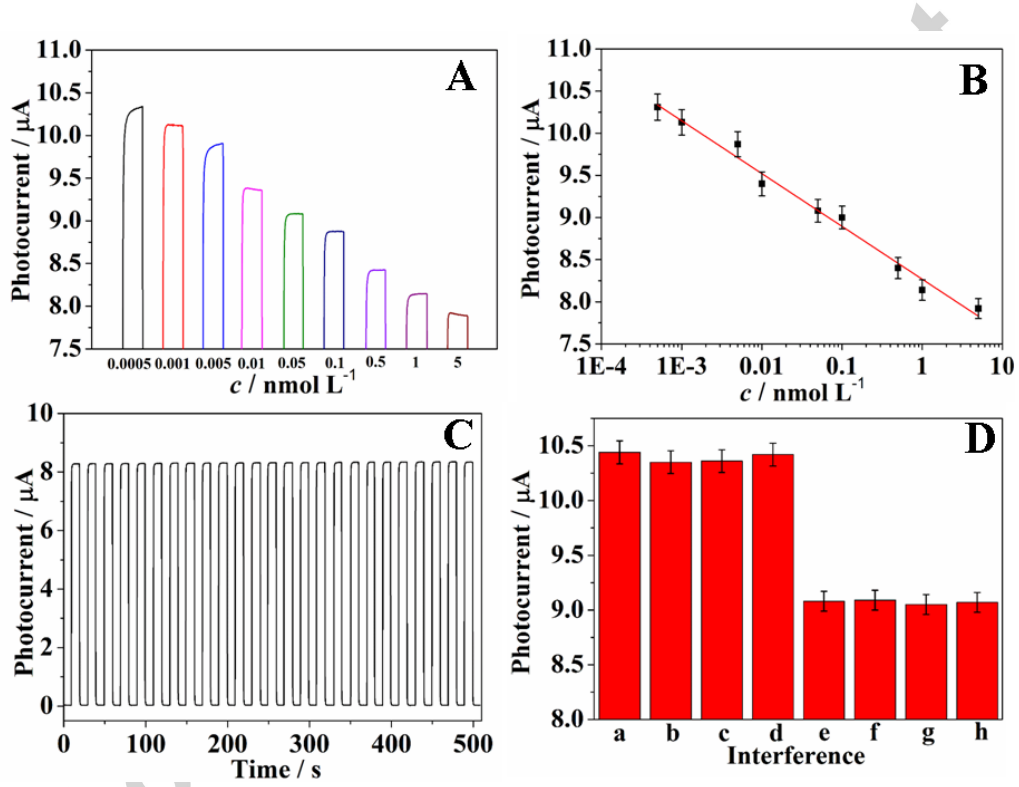

Fig. 6. (A) Time-based photocurrent response and (B) logarithmic calibration curve for PEC aptasensor for the detection of different concentrations of thrombin. (C) Photocurrent response of the PEC aptasensor under several on/off irradiation cycles for 500 s, $c_{thrombin}$= 1.0 nmol L^{-1}. (D) Selectivity of the proposed aptasensor to thrombin. (a) Blank, (b) Blank+5.0 nmol L^{-1} CEA, (c) Blank+5.0 nmol L^{-1} HlgG, (d) Blank+5.0 nmol L^{-1} glucose, (e) 0.05 nmol L^{-1} thrombin, (e) 0.05 nmol L^{-1} thrombin +5.0 nmol L^{-1} CEA, (f) 0.05 nmol L^{-1} thrombin +5.0 nmol L^{-1} HlgG, (g) 0.05

nmol L^{-1} thrombin +5.0 nmol L^{-1}+glucose. The applied potential was 0 V. The error bars in (B) and (D) showed the standard deviation of five replicate determinations.

The quantitative determination under the optimal conditions was carried out on the modified PEC electrodes incubated with a series of concentrations of thrombin. Because of the specific binding between thrombin aptamer (TBA) and thrombin, thrombin could bind on the blank electrode (ITO/(1%C_3N_4/TiO_2)/TBA/BSA). From the time-based photocurrent curves (Fig. 6A), the photocurrents decreased with the increase of thrombin concentration due to the biomolecular insulation properties of thrombin. Moreover, the photocurrent intensity decreased linearly with the logarithm of thrombin concentration in the range from 5×10^{-13} mol L^{-1} to 5×10^{-9} mol L^{-1} (Fig. 6B). The linear equation is $I = 8.2679 - 0.6268 \log (c_{thrombin}$, nmol $L^{-1})$ with a correlation coefficient of 0.9933. The detection limit is 1.2×10^{-13} mol L^{-1}, which is calculated according to literatures (Ren, et al., 2015). The linear range and detection limit of this new PEC aptasensor for thrombin are comparable to other sensing methods listed in Table S2 (ESI†). The facile PEC aptasensor is satisfactory.

Photocurrent response of the PEC aptasensor incubated with 1.0 nmol L^{-1} thrombin was estimated under 25 times on/off irradiation cycles for 500 s (Fig. 6C). There was little change of the photocurrent, supporting the good stability of the prepared C_3N_4/TiO_2 aptasensor. To assess the reproducibility of the present PEC aptasensor, five ITO electrodes were measured for the determination of 5.0 pmol L^{-1} thrombin, the photocurrents were 9.40 μA, 9.88 μA, 9.98 μA, 10.0 μA, 10.02 μA, respectively. The relative standard deviation (RSD) was 2.6%. For the determination of 1.0 nmol

L^{-1} thrombin with one sensor, the photocurrents of five measurements were 8.00 μA, 8.14 μA, 8.17 μA, 8.20 μA, 8.29 μA, respectively. The relative standard deviation (RSD) was 1.3%. These implied that the precision and reproducibility of the prepared PEC aptasensor were satisfactory.

Fig. 6D shows the selectivity of the PEC aptasensor for thrombin. The photocurrent responses were studied by mixing 0.05 nmol L^{-1} of thrombin with 5.0 nmol L^{-1} of carcinoembryonic antigen (CEA), 5.0 nmol L^{-1} human immune globulin G (HlgG) and 5.0 nmol L^{-1} glucose. No obvious interferential signal was generated from 5.0 nmol L^{-1} of CEA, HlgG or glucose in the presence or absence of thrombin, which illustrated excellent selectivity and specificity of the PEC aptasensor for thrombin.

3.5. Application of the aptasensor in human serum

Analysis of thrombin in human blood serum samples was performed by the standard addition method. Because no thrombin was found in the serum samples, the diluted serum (1:5 with pH 7.4 Tris-HCl buffer) was spiked with thrombin at different concentrations (10^{-12}, 10^{-11}, 10^{-10} and 10^{-9} mol L^{-1}). It can seen from Table S3 (ESI†), the relative standard deviation (RSD) was in the range of 1.9−4.6%, and the recoveries were in the range of 98.2−108.2%.

4. Conclusion

In summary, a novel PEC aptasensor platform for thrombin was facilely fabricated based on g-C_3N_4/TiO_2 with high visible-light PEC activity. The integration of TiO_2 NPs with g-C_3N_4 nanosheet contributed to the high visible-light PEC activity. Carboxyl functionalized thrombin aptamers were successfully bound to the

g-C_3N_4/TiO_2 modified ITO electrode. This proposed PEC aptasensor exhibited a wide detection range from 5.0×10^{-13} mol L^{-1} to 5.0×10^{-9} mol L^{-1} and a low detection limit of 1.2×10^{-13} mol L^{-1}. This simple, stable and low-cost PEC platform could be applied for sensing diverse targets by simple replacement with other aptamers.

Acknowledgments

This research was supported by the Natural Science Foundation of China (No. 21405059, 21203074, 21103071, 21375047), the Natural Science Foundation of Shandong Province (ZR2011BQ016), and Doctor Foundation of University of Jinan (XBS1311). QW thanks the Special Foundation for Taishan Scholar Professorship of Shandong Province and UJN (No. ts20130937). All of the authors express their deepest thanks.

References

An, Y.R., Tang, L.L., Jiang, X.L., Chen, H., Yang, M.C., Jin, L.T., Zhang, S.P., Wang, C.G., Zhang, W. 2010. Chem. Eur. J. 16, 14439−14446.

Anderson, S., Constable, E.C., Dare-Edwards, M. P., Goodenough, J.B., Hamnett, A., Seddon, K.R., Wright, R.D. 1979. Nature. 280, 571−573.

Asahi, R., Morikawa, T., Ohwaki, T., Aoki, K., Taga, Y. 2001. Science. 293, 269−271.

Brown, G.N., Birks, J.W., Koval, C.A. 1992. Anal. Chem. 64, 427−434.

Cheng, C., Huang, Y., Tian, X., Zheng, B., Li, Y., Yuan, H., Xiao, D., Xie, S., Choi, M.M.F. 2012. Anal. Chem. 84, 4754−4759.

Ellington, A.D., Szostak, J.W. 1990. Nature. 346, 818−822.

Eu, S., Hayashi, S., Umeyama, T., Oguro, A., Kawasaki, M., Kadota, N., Matano, Y., Imahori, H.

2007. J. Phys. Chem. C. 111, 3528−3537.

Freeman, R., Girsh, J., Willner, I. 2013. ACS Appl. Mater. Interfaces. 5, 2815−2834.

Grätzel, M. 2001. Nature. 414, 338−344.

Hermann, T., Patel, D.J. 2000. Science. 287, 820−825.

Hoffmann, M.R., Martin, S.T., Choi, W., Bahnemann, D.W. 1995. Chem. Rev. 95, 69−96.

Huang, Q., Tian, S., Zeng, D., Wang, X., Song, W., Li, Y., Xiao, W., Xie, C. 2013. ACS Catal. 3, 1477−1485.

Inturi, S.N.R., Boningari, T., Suidan, M., Smirniotis, P.G. 2014. Appl. Cataly. B: Environ. 144, 333−342.

Khabashesku, V.N., Zimmerman, J.L., Margrave, J. L. 2000. Chem. Mater. 12, 3264−3270.

Kuang, D., Ito, S., Wenger, B., Klein, C., Moser, J.E., Humphry-Baker, R., Zakeeruddin, S.M., Grätzel, M. 2006. J. Am. Chem. Soc. 128, 4146−4154.

Li, J.H., Yan, B.F., Shao, X.S., Wang, S.S., Tian, H.Y., Zhang, Q.Q. 2015. Appl. Surf. Sci. 324, 82−89.

Li, R.X., Liu, Y.X., Li, X.J., Zhang, S., Wu, D., Zhang, Y., Wei, Q., Du, Bin. 2014a. Biosens. Bioelectron. 62, 315−319.

Li, X.J., Zhang, X.Y., Ma, H.M., Wu, D., Zhang, Y., Du, B., Wei, Q. 2014b. Biosens. Bioelectron. 55, 330−336.

Li, Y.J., Ma, M.J., Zhu, J.J. 2012. Anal. Chem. 84, 10492−10499.

Liao, G., Chen, S., Quan, X., Yu, H., Zhao, H. 2012. J. Mater. Chem. 22, 2721−2726.

Linsebigler, A.L., Lu, G., Yates Jr, J.T. 1995. Chem. Rev. 95, 735−758.

Liu, J.H., Zhang, T.K., Wang, Z.C., Dawson, G., Chen, W. 2011. J. Mater. Chem. 21,

14398−14401.

Liu, Q., Zhang, J. 2013. Langmuir. 29, 3821−3828.

Liu, Y.X., Li, R.X., Gao, P.C., Zhang, Y., Ma, H.M., Yang, J.J., Du, B., Wei, Q. 2015. Biosens. Bioelectron. 65, 97−102.

Rajh, T., Dimitrijevic, N.M., Bissonnette, M., Koritarov, T., Konda, V. 2014. Chem. Rev. 114, 10177−10216.

Reddy, B.M., Lakshmanan, P., Khan, A. 2004. J. Phys. Chem. B. 108, 16855−16863.

Ren, K., Wu, J., Yan, F., Zhang, Y., Ju, H. 2015. Biosens. Bioelectron. 66, 345−349.

Schwinghammer, K., Mesch, M.B., Duppel, V., Ziegler, C., Senker, J., Lotsch, B.V. 2014. J. Am. Chem. Soc. 136, 1730−1733.

Sun, J.H., Zhang, J.S., Zhang, M.W., Antonietti, M., Fu, X.Z., Wang, X.C. 2012. Nat. Commun. 2, 1139.

Tang, X., Li, D. 2008. J. Phys. Chem. C. 112, 5405−5409.

Thomas, A., Fischer, A., Goettmann, F., Antonietti, M., Muller, J., Schlogl, R. Carlsson, J.M. 2008. J. Mater. Chem. 18, 4893−4908.

Thompson, T.L., Yates Jr, J.T. 2006. Chem. Rev. 106, 4428−4453.

Tong, Z., Yang, D., Xiao, T., Tian, Y., Jiang, Z. 2015. Chem. Eng. J. 260, 117−125.

Tu, W., Lei, J., Ding, L., Ju, H. 2009. Chem. Commun. 4227−4229.

Valentin, C.D., Pacchioni, G., Selloni, A. 2005. Chem. Mater. 17, 6656−6665.

Wang, G.L., Xu, J.J., Chen, H.Y., Fu, S.Z. 2009a. Biosens. Bioelectron. 25, 791−796.

Wang, X.C., Maeda, K., Thomas, A., Takanabe, K., Xin, G., Carlsson, J.M., Domen, K., Antonietti, M. 2009b. Nat. Mater. 8, 76−80.

Wang, Y., Wang, X.C., Antonietti, M. 2012. Angew. Chem. Int. Ed. Engl. 51, 68−89.

Xu, M., Han, L., Dong, S.J. 2013. ACS Appl. Mater. Interfaces. 5, 12533−12540.

Yan, S.C., Li, Z.S., Zou, Z.G. 2010. Langmuir. 26, 3894−3901.

Yu, J., Wang, S., Low, J., Xiao, W. 2013. Phys. Chem. Chem. Phys. 15, 16883−16890.

Yue, Z., Lisdat, F., Parak, W.J., Hickey, S.G., Tu, L., Sabir, N., Dorfs, D., Bigall, N.C. 2013. ACS Appl. Mater. Interfaces. 5, 2800−2814.

Zhang, L., Jing, D., She, X., Liu, H., Yang, D., Lu, Y., Li. J., Zheng, Z., Guo. L. 2014. J. Mater. Chem. A. 2, 2071−2078.

Zhao, W.W., Xu, J.J., Chen, H.Y. 2014. Chem. Rev. 114, 7421−7441.

Zhou, J., Zhang, M., Zhu, Y. 2015. Phys. Chem. Chem. Phys. 17, 3647−3652.

Highlights

► A novel g-C_3N_4/TiO_2 composite was synthesized with high visible-light activity.

► Synergistic effect between g-C_3N_4 and TiO_2 contributed to the high PEC activity.

► Carboxyl functionalized aptamer was first bound to the g-C_3N_4/TiO_2 electrode.

► The facile PEC aptasensor achieved sensitive detection of thrombin.